

Report Number 12/27

**The interplay between tissue growth and scaffold degradation in  
engineered tissue constructs**

by

**R. D. ODea, J. M. Osborne, A. J. El Haj, H. M. Byrne, S. L.  
Waters**



Oxford Centre for Collaborative Applied Mathematics  
Mathematical Institute  
24 - 29 St Giles'  
Oxford  
OX1 3LB  
England



# The interplay between tissue growth and scaffold degradation in engineered tissue constructs.

R. D. O'Dea\*, J. M. Osborne\*, A. J. El Haj, H. M. Byrne & S. L. Waters

Received: date / Accepted: date

**Abstract** *In vitro* tissue engineering is emerging as a potential tool to meet the high demand for replacement tissue, caused by the increased incidence of tissue degeneration and damage. A key challenge in this field is ensuring that the mechanical properties of the engineered tissue are appropriate for the *in vivo* environment. Achieving this goal will require detailed understanding of the interplay between cell proliferation, extracellular matrix (ECM) deposition and scaffold degradation.

In this paper, we use a mathematical model (based upon a multiphase continuum framework) to investigate the interplay between tissue growth and scaffold degradation during tissue construct evolution *in vitro*. Our model accommodates a cell population and culture medium, modelled as viscous fluids, together with a porous scaffold and ECM deposited by the cells, represented as rigid porous materials. We focus on tissue growth within a perfusion bioreactor system, and investigate how the predicted tissue composition is altered under the influence of (i) differential interactions between cells and the supporting scaffold and their associated ECM, (ii) scaffold degradation, and (iii) mechanotransduction-regulated cell proliferation and ECM deposition.

Numerical simulation of the model equations reveals that scaffold heterogeneity typical of that obtained from  $\mu$ CT scans of tissue engineering scaffolds can lead to significant variation in the flow-induced mechanical stimuli

---

\*Joint first authors

---

R. D. O'Dea  
School of Science and Technology, Nottingham Trent University, Clifton Campus, Nottingham, NG11 8NS, UK  
Tel.: +44 (0)115 848 8050  
Fax.: +44 (0)115 848 6636  
E-mail: reuben.odea@ntu.ac.uk

J. M. Osborne  
Department of Computer Science, University of Oxford, Wolfson Building, Parks Road, Oxford, OX1 3QD, UK  
Tel.: +44 (0)1865 273525  
Fax.: +44 (0)1865 273583  
E-mail: James.Osborne@cs.ox.ac.uk

A. J. El Haj  
Institute for Science & Technology in Medicine, Keele University, Guy Hilton Research Centre, Stoke-on-Trent ST4 7QB, UK  
Tel.: +44 (0)1782 554 605  
Fax.: +44 (0)1782 747319  
E-mail: a.j.el.haj@bemp.keele.ac.uk

H. M. Byrne  
Oxford Centre for Collaborative Applied Mathematics, Mathematical Institute, Gibson Building, Oxford, OX2 6HA, UK  
Department of Computer Science, University of Oxford, Wolfson Building, Parks Road, Oxford, OX1 3QD, UK Tel.: +44 (0)1865 615149  
Fax.: +44 (0)1865 615164  
E-mail: Helen.Byrne@maths.ox.ac.uk

S. L. Waters  
Oxford Centre for Industrial and Applied Mathematics,  
Mathematical Institute, 24-29 St Giles', Oxford, OX1 3LB, UK  
Tel.: +44 (0)1865 280141  
Fax.: +44 (0)1865 270515  
E-mail: waters@maths.ox.ac.uk

experienced by cells seeded in the scaffold. This leads to strong heterogeneity in the deposition of ECM. Furthermore, preferential adherence of cells to the ECM in favour of the artificial scaffold appears to have no significant influence on the eventual construct composition; adherence of cells to these supporting structures does, however, lead to cell and ECM distributions which mimic and exaggerate the heterogeneity of the underlying scaffold. Such phenomena have important ramifications for the mechanical integrity of engineered tissue constructs and their suitability for implantation *in vivo*.

**Keywords** Multiphase · Scaffold heterogeneity · Perfusion bioreactor

## 1 Introduction

Mathematical modelling of tissue growth is a wide field of research, aiming to provide a more complete understanding of the myriad biological and biophysical processes that contribute to tissue growth. Such theoretical models underpin the emerging field of *in vitro* tissue engineering, which, by the creation of replacement tissue in the laboratory, has the potential to alleviate the shortage of replacement tissue available for implantation into patients. A typical method for generating such implants entails seeding a biodegradable porous scaffold with cells; subsequent incubation in a bioreactor allows the cells to colonise the porous scaffold (termed a tissue construct). On implantation, the degrading scaffold is replaced by extracellular materials such as collagen and proteoglycans, which are laid down by the cells (Freed *et al*, 1994). Ensuring that the rates of nascent tissue growth and scaffold degradation (*e.g.* due to hydrolysis) are appropriately matched is therefore crucial in maintaining the mechanical integrity of the construct, a factor of especial importance for load-bearing constructs, such as bone implants (Wu and Ding, 2004). The biological processes which contribute to tissue construct growth operate on disparate spatio-temporal scales and range from intracellular gene networks to tissue-level mechanics; reviews are given by Curtis and Riehle (2001), Cowin (2000, 2004), Sipe (2002) and Burdick and Mauck (2010). In this paper, we concentrate on a tissue-scale description of tissue growth, and employ a continuum model to focus on the way in which the properties of the supporting scaffold influence the structure of the resulting tissue construct.

In addition to the scaffold's mechanical properties, its chemical features are of great importance. For example, most cell types are anchorage-dependent, their growth being affected by interactions between a substrate or deposited extracellular matrix (ECM); the surface chemistry of the scaffold crucially affects such interactions. Adherence to polymer scaffolds commonly employed in tissue engineering applications is mediated by adsorption of deposited ECM molecules onto the scaffold surface or by, for instance, artificially embedded cell recognition molecules (Freed and Vunjak-Novakovic, 1998; Nikolovski and Mooney, 2000). The type and density of such molecules may vary dramatically throughout the scaffold due to, *e.g.*, inhomogeneous ECM deposition, leading to spatial variations in cell adhesion characteristics, or preferential adherence to ECM or other deposited materials over artificial scaffolds.

Controlling the biochemical environment of cells (both with respect to nutrient/oxygen delivery and the provision of growth factors and other cell-signalling molecules) is key to producing constructs of a size appropriate for implant, while minimising the necrotic core which often forms at the centre of tissue constructs in static culture. To this end perfusion bioreactors are frequently employed, which exploit advection of culture medium to enhance mass transport. This approach also provides mechanical stimulation to cells contained within a porous scaffold via culture medium flow-induced shear stress, and can allow for the addition of cyclical compressive loads. For example, El-Haj and coworkers have developed a perfusion/compression bioreactor system which comprises a poly(L-lactic acid) (PLLA) scaffold, through which culture medium is perfused via a peristaltic pump; macroscale compression of the scaffold may also be effected by the addition of a piston (Haj *et al*, 1990). (The layout of the bioreactor system in the absence of macroscale compression is depicted in Figure 1.) Cells contained within a porous scaffold are therefore subjected to culture medium flow-induced shear stress and macroscale strain, in addition to mechanical interactions which exist between adjacent cells, such as contact inhibition, and between cells and scaffold/ECM. Other strategies for applying mechanical stimulation to tissue engineered constructs are reviewed by Martin *et al* (2004) and Cartmell and El Haj (2005). The process by which such stimuli are integrated into the cellular response, for example, in terms of its proliferative behaviour, is known as mechanotransduction. The biochemical and biomechanical environment required for optimum growth is specific to the tissue under consideration; bespoke bioreactors are therefore required to provide appropriate cues for different tissue engineering applications. Well-studied examples include osteocytes (terminally-differentiated bone cells), which are known to be sensitive to fluid shear stress (Bakker *et al*, 2004a); and chondrocytes, whose metabolism and maintenance of ECM integrity are regulated by mechanical stress (Urban, 1994; Wang *et al*, 2010). Indeed, in Haj *et al* (1990) attention focussed on the influence of such mechanical stimulation on bone tissue growth.

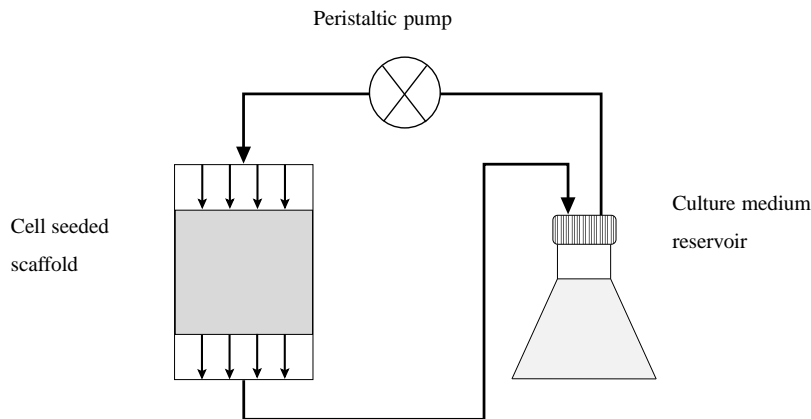


**Fig. 1** Layout of the bioreactor system of Haj et al (1990).

In what follows, we employ a mathematical model relevant to perfusion bioreactor systems in which cells are cultivated within a porous scaffold. Our formulation accommodates the cells' progression from a proliferative to an apoptotic phenotype, via an ECM depositing phase, in response to changes in the local cell volume fraction (modelling, *e.g.*, contact inhibition; a methodology for accommodating mechanotransduction-mediated cell proliferation in response to a range of mechanical stimuli is given in O'Dea et al (2008, 2010) and Osborne et al (2010)), as well as considering in detail the interactions between the cells and their supporting structures.

A variety of approaches has been employed to model tissue growth, their respective benefits depending on the specific application under consideration. Here, we study an extension to a recently-developed continuum model (O'Dea et al, 2010) in which we consider the evolution of the spatial distribution of PLLA scaffold and ECM density. We employ a multiphase formulation which enables us to incorporate interactions between the many constituent materials which comprise biological tissue; we model explicitly cell-cell and cell-scaffold/ECM interactions as well as mass transfer between phases (representing cell proliferation, ECM deposition and scaffold degradation). Such multiphase approaches have been widely employed in industrial applied mathematics (Drew and Segel, 1971) and, more recently, modelling of tumour growth and *in vitro* tissue engineering processes; examples include Breward et al (2002), Byrne and Preziosi (2003), Franks and King (2003), Araujo and McElwain (2005), Lemon et al (2006), Lemon and King (2007), Wilson et al (2007), O'Dea et al (2008, 2010), Osborne et al (2010), and references therein. Reviews are given by, *e.g.*, Preziosi and Tosin (2009) and O'Dea et al (2011).

In O'Dea et al (2010), tissue growth within a perfusion bioreactor was modelled, using a three-phase continuum model in a 2D channel geometry. In common with multiphase models of similar biological systems (Landman and Please, 2001; Byrne and Preziosi, 2003; Franks and King, 2003; Lemon et al, 2006), the cells and associated ECM were represented as a viscous fluid phase that is distinct from the culture medium; and the porous scaffold was modelled as a rigid porous medium. Two factors of key importance to modelling the growth and adaptation of engineered tissue constructs were investigated: (i) cell-cell and cell-scaffold interactions and, (ii) mechanotransduction mechanisms. The formulation was simplified via the long-wavelength limit (in which the bioreactor's aspect ratio is assumed to be small) and by considering constant, spatially-homogeneous scaffold porosity. Numerical simulation of the model equations (validated by analytic solutions obtained in the limit of asymptotically-small cell volume fraction), revealed that inclusion of cell-cell and cell-scaffold interactions leads to significant differences in the extent to which the cell population colonises the scaffold, depending upon the relative importance of cell aggregation and repulsion. It was further shown that the composition of the resulting construct was strongly influenced by whether cell proliferation and ECM deposition were regulated by mechanical stimulation related to the cell volume fraction, pressure or shear stress. Employing two-dimensional finite element simulations, Osborne et al (2010) demonstrated that, when considering total tissue yield, the long-wavelength limit of O'Dea et al (2010) provides an excellent approximation to the full two-dimensional model, even for relatively large values of bioreactor aspect ratio. However, this work further demonstrated that mechanotransduction-mediated tissue growth can lead to significant two-dimensional spatial variation of tissue density, a feature which is not captured by the long-wavelength limit. The authors concluded that, while spatial effects in two- or three-dimensions cannot be ignored in comprehensive models of tissue growth, its relative simplicity makes the long-wavelength model a natural framework with

which to estimate parameters relevant to specific bioreactor systems, for subsequent use in more complex two- or three-dimensional models.

Whilst the inclusion of the scaffold phase is a significant departure from two-fluid models (see, for example, Franks and King (2003)) since interactions between the rigid scaffold and cell phases are explicitly modelled, a key assumption of O'Dea et al (2010) and Osborne et al (2010) is that the scaffold phase is spatially-homogeneous and constant in time, leading to significant simplification of the model formulation. Lemon and King (2007) considered non-uniform porosity only near the edge of the scaffold; however,  $\mu$ CT scans of porous scaffolds typically employed in tissue engineering applications indicate significant heterogeneity throughout the scaffold, as well as inhomogeneous deposition of extracellular materials (see, *e.g.*, Yang and El Haj (2006) for a discussion of tissue engineering scaffolds). Figure 2(a) shows a typical scaffold of the type employed in Haj et al (1990); Figure 2(b) shows experimental data indicating the cross section-averaged scaffold volume fraction along the axial length of such a scaffold, together with that following culture, indicating the level of mineralisation by osteocytes during culture. Such heterogeneity in scaffold density is likely to have implications for the mechanical properties of the resulting tissue construct, these considerations being especially important where the tissue is to be load-bearing, as is the case for cartilage or bone tissue: areas of weakness in implanted tissues may fail under physiological loading. For this reason, we aim to use our model to study how experimentally-relevant spatial variations in scaffold porosity may influence construct composition, and to indicate its importance in the generation of viable replacement tissue.

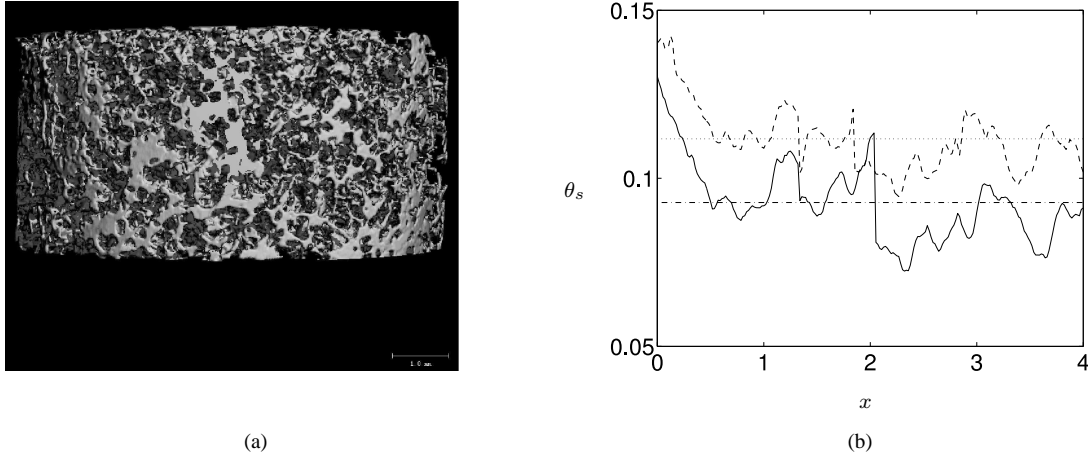


**Fig. 2** (a) A typical cylindrical PLLA scaffold employed in the bioreactor system of Haj et al (1990). The scale bar indicates 1mm; dimensions are: 9mm (diameter), 4mm (height). (b) Typical variation in the cross section-averaged scaffold density (represented by the scaffold volume fraction,  $\theta_s$  at axial position  $x$ ) before and after culture, observed experimentally in such a scaffold. The initial scaffold density is represented by “—” (with average “.....”) and the final scaffold by “- - -” (with average “...”).

A simple study considering scaffold degradation and ECM deposition is given by Haider et al (2010), in which the (spatially-independent) evolution of the total scaffold and ECM density is calculated using a phenomenological mixture model; specific consideration is given to scaffold-ECM linkage. The study concludes that the initial scaffold density will affect significantly the resulting construct's mechanical properties. More complex models, considering spatial dependence, include Kelly and Prendergast (2003), in which a core of underdeveloped tissue in a poroelastic model of cartilage tissue was considered, showing that construct inhomogeneity dramatically reduces its mechanical integrity. Optimal design of porous scaffolds was discussed in Adachi et al (2006) where the interplay between tissue growth and scaffold degradation, as well as the scaffold microstructure, was considered. Sanz-Herrera et al (2008) developed a multiscale model to investigate the interplay between scaffold design parameters and bone tissue regeneration. By constructing solutions using finite element methods, the authors indicated that bone regeneration increases with scaffold stiffness and mean pore size. Byrne et al (2007) considered the influence of scaffold porosity and degradation rate on *in vitro* bone tissue growth; mechanotransduction-regulated differentiation of stem cells to fibroblasts, chondrocytes and osteoblasts was also accommodated, each phenotype displaying different migration and material properties. A random walk model for cell movement within a poroelastic scaffold (whose deformation was simulated via a finite element method) was used to compute the tissue composition. The study concluded that under low load, high porosity and stiffness, together with an intermediate

scaffold degradation rate, stimulate increased bone tissue generation; to prevent collapse of the scaffold under high load, a reduced degradation rate is required.

Due to the nature of the problems investigated (three-dimensional scaffolds with specific pore geometry, deformation, flow, scaffold mechanical properties), many of the studies mentioned above give rise to complex systems of coupled PDEs, which are heavily reliant on numerical investigation. In this study, we demonstrate that considerations relevant to biological tissue growth may be accommodated within a continuum model, amenable to asymptotic simplification; we extend our earlier work O'Dea et al (2010) by relaxing the assumption of constant, homogeneous scaffold porosity, and employ the resulting model to investigate the interplay between scaffold degradation and nascent tissue growth in a perfusion bioreactor. Our model incorporates a cell population and culture medium, each represented as a viscous fluid, as well as both a PLLA scaffold and ECM deposited by the cells, modelled as rigid porous phases. This approach allows spatio-temporal variations in cell-scaffold and cell-ECM interactions, realistic scaffold porosity distributions (informed by experimental data), scaffold degradation, and mechanotransduction-regulated cell proliferation and ECM deposition to be accommodated.

In the limit of asymptotically-small bioreactor aspect ratio, the resulting model simplifies to three nonlinear differential equations. Via this formulation, we seek to provide a more comprehensive description of *in vitro* tissue growth, while remaining within a simplified modelling framework. Our investigations reveal that spatial inhomogeneity in scaffold volume fraction strongly influences the cells' mechanical environment, leading to inhomogeneous cell proliferation and ECM deposition. Further, our model suggests that preferential adherence to ECM in favour of the PLLA scaffold has no significant influence on the eventual construct composition; we therefore conclude that such additional mathematical complexity is unnecessary, so that simplified models, in which cells interact uniformly with their supporting structures, may be employed to describe biological tissue growth. Lastly, by associating scaffold degradation with detrimental effects on the construct's material properties (*e.g.*, increased susceptibility to failure under *in vivo*-like loading conditions), which are mitigated by deposition of ECM and other extracellular materials, we indicate that careful manipulation of the rate of PLLA scaffold degradation is required in order to maintain the mechanical integrity of constructs and their suitability for implantation.

The remainder of the paper is organised as follows. In §2, the multiphase model of O'Dea et al (2010) is summarised, and extended by the addition of spatial and temporal variation in scaffold and ECM volume fractions, and the resulting governing equations and boundary conditions are stated (a detailed derivation is provided in the Appendix). In §3, numerical simulations of the model equations are presented and the importance of scaffold degradation, ECM deposition and heterogeneity in scaffold porosity on construct composition is investigated. §4 provides a summary of the results contained in the preceding sections and a discussion of their implications for *in vitro* tissue engineering, together with suggestions for future avenues of investigation.

## 2 Model formulation

In this section, we present a multiphase model which describes the growth of a tissue construct within a nutrient-rich perfusion bioreactor. The bioreactor under consideration is illustrated in Figure 1 and comprises a cell-seeded porous scaffold within a culture medium-filled cylinder, through which a flow is driven (see Haj et al (1990) and O'Dea et al (2010) for details). The key modelling assumptions are summarised below and the resulting equations, together with appropriate boundary and initial conditions, are stated. The derivation of these equations is summarised in the Appendix for completeness. The interested reader is directed to O'Dea et al (2010) and references therein for a detailed discussion of the modelling considerations embodied by these equations when variations in scaffold fraction are neglected, and the ECM is encompassed within the cell phase.

For simplicity, we view the perfusion bioreactor as a two-dimensional channel (we expect results for an axisymmetric cylinder to be qualitatively similar) containing a mixture of four interacting phases. The cell population and culture medium are modelled as distinct viscous fluids, and rigid porous phases represent the PLLA scaffold and the ECM. The interplay between cell proliferation, ECM deposition and scaffold degradation is captured by mass exchange between the relevant phases, effected by the specification of mass transfer functions which account for the influence of mechanotransduction on cell proliferation and ECM deposition.

The mechanical interactions between phases comprise interphase viscous drag (proportional to differences in phase velocity) and active forces. The latter enter the governing equations via prescribed contributions to the cell phase pressure, arising due to cell-cell interactions and traction between the cell and scaffold or ECM phases, respectively. Interactions between the culture medium and scaffold/ECM phases are assumed to involve only viscous drag.

The mechanical interactions in this four phase formulation are simplified by lumping the rigid PLLA scaffold and ECM together into a single phase, referred to as the 'substrate' (a similar approach is used by Lubkin and

Jackson (2002)). We nevertheless track individually the evolution of the PLLA scaffold and ECM volume fractions, which allows us to distinguish between cell-scaffold and cell-ECM interactions. From a mechanical point of view, this model may therefore be thought of as a three phase system, differing from O'Dea et al (2010) in the sense that the scaffold and ECM phases are mechanically identical, but chemically distinct. We further assume that the bioreactor has a small aspect ratio, so that significant simplification of the governing equations can be achieved.

## 2.1 Dimensionless model equations and boundary conditions

We consider a 2D Cartesian coordinate system  $\mathbf{x} = (x, y)$ , in which the bioreactor is assumed to occupy the dimensionless region  $0 \leq x \leq 1, 0 \leq y \leq h \ll 1$ , and within which the PLLA scaffold phase is localised in the region  $a \leq x \leq b$  (where  $0 < a < b < 1$ , and  $a, b - a, 1 - b \gg h$ ). We assume that all dependent variables are functions of  $\mathbf{x}$  and dimensionless time,  $t$ .

The volume fractions of the cell, culture medium, PLLA scaffold and ECM phases are denoted by  $\theta_n, \theta_w, \theta_s$  and  $\theta_e$ , respectively; and the substrate phase  $\Theta$  is defined by

$$\Theta = \theta_s + \theta_e. \quad (1)$$

The dimensionless velocities and pressures of the cell and culture medium phases are denoted  $\mathbf{u}_i = (u_i, v_i)$  and  $p_i$  ( $i = n, w$ ; the rigidity of the PLLA scaffold and ECM implies  $\mathbf{u}_s = \mathbf{u}_e = \mathbf{0}$  and  $p_s = p_e = 0$ ). Cell proliferation, scaffold degradation and ECM deposition are captured via material transfer functions  $S_i$  which we specify below. The governing equations are stated below in dimensionless form.

The model is constructed by considering mass and momentum balances for each phase, assuming that the fluid phases are incompressible with equal density, and by neglecting inertial effects (details of the model derivation and nondimensionalisation are provided in the Appendix). Assuming that the bioreactor aspect ratio is asymptotically small, and employing the momentum balance equations, together with the no-voids condition,  $\sum_i \theta_i = 1$ , it is straightforward to show that the flow is unidirectional and that the pressure and volume fraction of each phase are functions of  $x$  and  $t$ . By eliminating dependent variables, the system may be reduced to the following differential equations for  $\theta_s, \theta_e, \theta_n$  and  $p_w$ :

$$\frac{\partial \theta_s}{\partial t} = S_s, \quad (2)$$

$$\frac{\partial \theta_e}{\partial t} = S_e, \quad (3)$$

$$\frac{\partial \theta_n}{\partial t} + \frac{1}{12\mu_n} \frac{\partial}{\partial x} \left( \theta_n \frac{\partial p_w}{\partial x} \right) = S_n, \quad (4)$$

$$\begin{aligned} \frac{\partial}{\partial x} \left\{ (\theta_n + \mu_n(1 - \theta_s - \theta_e - \theta_n)) \frac{\partial p_w}{\partial x} - p_w \frac{\partial}{\partial x} (\theta_e + \theta_s) \right\} \\ + \frac{\partial}{\partial x} \left\{ \frac{\partial(\theta_n^2 \Sigma)}{\partial x} + \theta_n \frac{\partial((\theta_e + \theta_s)\psi)}{\partial x} \right\} = 0, \end{aligned} \quad (5)$$

in which  $\mu_n$  is the relative viscosity of the cell and culture medium phases, and  $\Sigma$  and  $\psi$  capture active forces that exist between adjacent cells, and between cells and the substrate.

Equations (2)–(4) are the mass conservation equations for the PLLA scaffold, ECM and cell phases. The latter states that the rate of change of the cell volume fraction  $\theta_n$  is due to advection and the proliferation of cells; PLLA scaffold and ECM evolution is due to deposition of ECM and scaffold degradation only, and therefore  $\theta_e, \theta_s$  have an implicit spatial dependence. Equation (5) embodies conservation of mass for the multiphase mixture. In view of Equation (1), Equations (2)–(5) may be recast as a set of three nonlinear differential equations for  $\Theta, \theta_n$  and  $p_w$ , with (2) and (3) replaced with

$$\frac{\partial \Theta}{\partial t} = S_\Theta; \quad S_\Theta = S_s + S_e, \quad (6)$$

reflecting the pseudo-three phase nature of the model.

Equations (4) and (5) are closed by imposing the following boundary conditions:

$$\frac{\partial \theta_n}{\partial x} = 0 \quad \text{at} \quad x = 0, 1, \quad (7)$$

$$p_w = P_U \quad \text{at} \quad x = 0, \quad (8)$$

$$p_w = P_D \quad \text{at} \quad x = 1, \quad (9)$$



where  $P_U$  and  $P_D$  are the imposed up- and downstream pressures; initial conditions for  $\theta_n$ ,  $\theta_s$  and  $\theta_e$  are specified subsequently.

In this paper, we consider the influence of scaffold properties on tissue construct growth and composition by examining the interplay between scaffold degradation and nascent tissue growth under the influence of biologically-relevant cell-substrate interactions, and mechanotransduction-regulated cell proliferation and ECM deposition. These phenomena are captured by the interaction functions  $\Sigma$ ,  $\psi$  and the material transfer functions  $S_n$ ,  $S_e$  and  $S_s$  which are specified in terms of the dependent variables below.

## 2.2 Cell-cell and cell-scaffold interactions

The functions  $\Sigma$  and  $\psi$  describe respectively mechanical interactions between cells and between cells and their substrate; examples of relevant interactions include cell-cell and cell-substrate adhesion, and, in the case of motile cells such as fibroblasts, tractions between cells and their substrate.

Following Lemon et al (2006) and O'Dea et al (2010), we prescribe  $\Sigma$  and  $\psi$  as follows:

$$\Sigma = -\nu + \frac{\delta_a \theta_n}{(1 - \Theta - \theta_n)}, \quad \psi = -\chi + \frac{\delta_b \theta_n}{(1 - \Theta - \theta_n)}, \quad (10)$$

wherein  $\nu$ ,  $\chi$ ,  $\delta_a$  and  $\delta_b$  account for the cells' tendency to aggregate, their affinity for the substrate and the strength of the repulsive forces between cells and between cells and substrate. We remark that in this simplified formulation, cell-scaffold and cell-ECM interactions are lumped together in (10); however, as detailed below, we exploit our knowledge of the separate evolution of  $\theta_s$  and  $\theta_e$  to distinguish between cell-scaffold and cell-ECM interactions.

As discussed in §1, cell adhesion to polymer scaffolds is mediated by adsorption of ECM molecules, or the embedding of specific cell recognition molecules, into the scaffold surface (Freed et al, 1994; Nikolovski and Mooney, 2000). Since the type and density of such molecules can vary markedly, depending on the surface chemistry of the polymer, it is reasonable to expect that cells preferentially adhere to their extracellular matrices rather than synthetic substitutes. In this study, we aim to understand how such a disparity in cell-scaffold and cell-ECM interactions may influence the composition of the developing construct. We achieve this by comparing simulation results for the case  $\chi = \text{constant}$  with those obtained for  $\chi = \chi(\theta_e)$ , so that the affinity of the cells for the substrate phase depends on how much ECM has been deposited on the PLLA substrate; for simplicity, the remaining interaction terms  $\nu$ ,  $\delta_a$  and  $\delta_b$  are treated as fixed parameters.

We specify  $\chi(\theta_e)$  as follows:

$$\chi(\theta_e) = \chi_0 + \frac{\chi_1 - \chi_0}{2} (\tanh(g_1(\theta_e - \theta_{e_0})) + 1). \quad (11)$$

For suitably large  $g_1 = \text{constant}$ , this represents a smoothed switch between the values  $\chi_0$  (the affinity between cells and scaffold in the absence of deposited ECM) and  $\chi_1 > \chi_0$  (the elevated affinity due to ECM accumulation);  $\theta_{e_0}$  is the threshold level of ECM deposition at which this change occurs. In the limit  $g_1 \rightarrow \infty$ , the progression between  $\chi_0$  and  $\chi_1$  approximates a step function.

## 2.3 Mechanotransduction-mediated growth

The cells' response to biomechanical stimuli is accounted for by appropriate specification of the mass transfer rates  $S_i$  ( $i = n, e, s$ );  $S_w$  is chosen to ensure conservation of mass. Stimuli relevant to tissue engineering applications include contact inhibition, residual stress caused by tissue growth (Fung, 1991; Skalak et al, 1996; Roose et al, 2003; Chaplain et al, 2006; Holzapfel and Ogden, 2006) and the local fluid dynamics, such as the local hydrostatic pressure (Roelofsen et al, 1995; Klein-Nulend et al, 1995) or fluid shear stress (You et al, 2000, 2001; Bakker et al, 2004b; Han et al, 2004; Yourek et al, 2004).

The focus of the current study is the interplay between scaffold degradation, tissue growth and cell-cell/cell-substrate interactions; for brevity, we restrict attention to cases in which cell proliferation and ECM deposition are regulated by contact inhibition and/or residual stress. (Consideration of the influence of a wider range of mechanical stimuli is given in O'Dea et al (2010) and Osborne et al (2010).) We represent such regulation in our model by introducing net cell proliferation and ECM deposition rates  $\kappa^n$ ,  $\kappa^e$  which depend upon the local cell volume fraction; the PLLA scaffold is assumed to degrade at a constant rate  $k_d^s$ . We identify three distinct cellular responses to the local cell volume fraction: a proliferative phenotype, an ECM-depositing phenotype and an apoptotic phenotype, for each of which  $\kappa^n$ ,  $\kappa^e$  take different values. The progression from one phenotype to the next occurs at

threshold densities  $\theta_{n_1}$  and  $\theta_{n_2}$  ( $0 < \theta_{n_1} < \theta_{n_2}$ ). Functional forms for  $\kappa^n$  and  $\kappa^e$  are specified below and depicted in Figure 3.

$$S_n(\theta_n) = \theta_n \kappa^n(\theta_n), \quad S_e(\theta_n) = \theta_n \kappa^e(\theta_n), \quad S_s(\theta_s) = -k_d^s \theta_s, \quad (12)$$

$$\kappa^n(\theta_n) = k_m^n - \frac{k_m^n + k_d^n}{2} (\tanh(g_2(\theta_n - \theta_{n_2})) + 1), \quad (13)$$

$$\kappa^e(\theta_n) = \frac{k_m^e}{2} (\tanh(g_2(\theta_n - \theta_{n_1})) - \tanh(g_2(\theta_n - \theta_{n_2}))). \quad (14)$$

Equations (12)–(14) embody the following assumptions: (i) cells proliferate at a constant rate  $k_m^n$  until the cell volume fraction exceeds  $\theta_{n_2}$ , when they become apoptotic (with death rate  $k_d^n$ ); (ii) at intermediate values, the cells also deposit ECM at a rate  $k_m^e$ . As in Equation (11), in the limit  $g_2 \rightarrow \infty$ ,  $\kappa^n$  and  $\kappa^e$  are piecewise-constant and the progression between phenotypes obeys a step function; in what follows, we choose  $g_2 = g_1 = 100$ .

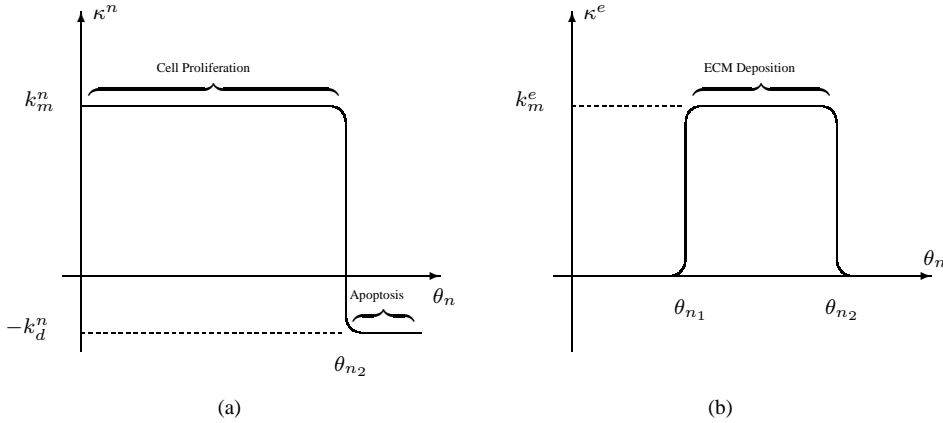


**Fig. 3** (a) The net cell proliferation rate,  $\kappa^n$ , and (b) the ECM deposition rate,  $\kappa^e$ , representing phenotypic progression in response to the local cell volume fraction  $\theta_n$ . The dimensionless parameters  $k_m^n$  and  $k_m^e$  represent the rate of cell proliferation and ECM deposition whilst  $k_d^n$  represents the rate of cell death. The thresholds are  $\theta_{n_1}$  and  $\theta_{n_2}$ .

## 2.4 Initial conditions

Tissue engineers employ a number of different techniques to seed porous scaffolds with cells. Here we consider static seeding, in which a suspension of cells is injected onto the surface of, or into, the scaffold, leading to an initial cell population which is localised near the point of injection. Following O'Dea et al (2010) and Osborne et al (2010), we prescribe:

$$\theta_n(x, 0) = \frac{\hat{n}_s}{2} (\tanh(g_3(x - \alpha)) - \tanh(g_3(x - \beta))), \quad (15)$$

where  $\hat{n}_s$  is the maximum initial cell volume fraction, and  $x = \alpha$  and  $x = \beta$  represent the left and right hand edges of the localised cell distribution within the scaffold region (*i.e.*  $0 < a < \alpha < \beta < b < 1$ ), near which  $g_3$  governs the spatial gradient of  $\theta_n$ . In what follows, we fix  $a = 0.25$ ,  $b = 0.75$ ,  $\hat{n} = 0.2$ ,  $\alpha = 0.4375$ ,  $\beta = 0.5625$ , and  $g_3 = 50$  without loss of generality.

Assumptions of uniform porosity have been employed in previous studies of *in vitro* tissue growth (Lemon et al, 2006; O'Dea et al, 2010; Osborne et al, 2010); however, the structure of scaffolds typically employed in such tissue engineering systems is highly heterogeneous (see Figure 2). To determine the influence of such heterogeneity on construct evolution, we compare the predicted construct composition resulting from two separate initial conditions for the PLLA scaffold:

$$\theta_s(x, 0) = \begin{cases} \theta_s^{\text{ideal}} & \text{for } a \leq x \leq b \\ 0 & \text{otherwise} \end{cases}, \quad \theta_s(x, 0) = \begin{cases} \theta_s^{\mu CT}(x) & \text{for } a \leq x \leq b \\ 0 & \text{otherwise} \end{cases}. \quad (16 a, b)$$

We set  $\theta_s^{\text{ideal}} = 0.0928$ , this being the average initial scaffold volume fraction shown in Figure 2, so that the former initial condition represents a scaffold of width  $(b - a)$  and uniform porosity  $\approx 91\%$ . The choice  $\theta_s^{\mu CT}(x)$  denotes the spatially-varying initial experimental data shown in Figure 2. In all cases, the initial ECM distribution is specified as

$$\theta_e(x, 0) = 0. \quad (17)$$

### 3 Numerical results

In this section, we present numerical simulations of Equations (2)–(5), subject to the boundary conditions (7)–(9). Employing Equations (10)–(14), and the initial conditions (15)–(17), we investigate how the cells’ response to their environment (especially their interactions with the underlying substrate) influences the composition of the resulting tissue construct.

The numerical scheme that we use and its validation are described in Osborne and Whiteley (2010) and Osborne et al (2010) and so we do not include details here. To summarise, Equation (5) is solved for  $p_w$  using  $\theta_n$ ,  $\theta_s$  and  $\theta_e$  from the previous timestep (with a linear finite element approximation for  $p_w$ ); employing this solution for  $p_w$ , the remaining dependent variables,  $\theta_n$ ,  $\theta_e$  and  $\theta_s$  are updated by applying to (2)–(4) an implicit Euler method, together with linear finite element approximations. For numerical convenience, we include a diffusive term, with constant diffusivity  $D$  (here we use  $D = 0.001$ ), in Equation (4) which converts it to a second order parabolic equation. With  $D > 0$  we need not track explicitly the sharp interface which is evident when  $D = 0$ . Such artificial diffusion has a negligible effect on the solution behaviour VonNeumann and Richtmyer (1950). Model parameter values are selected to illustrate the behaviour of the model and are similar to those employed in O’Dea et al (2010) and Osborne et al (2010); the specific values chosen are summarised in Table 1 and repeated in the relevant figure captions.

**Table 1** Summary of dimensionless parameters employed in numerical simulations.

General parameters		
$P_D$	downstream applied pressure	0.1
$P_U$	upstream applied pressure	0.3
$\mu_n$	ratio of dimensional viscosities $\mu_n^*/\mu_w^*$	1.3
$a$	upstream boundary of scaffold	0.25
$b$	downstream boundary of scaffold	0.75
$D$	cell volume fraction diffusivity	0.001
Cell-substrate interaction parameters		
$\nu$	cell aggregation parameter	0.05
$\delta_a$	intrapphase repulsion parameter	0.05
$\chi_0$	minimum substrate affinity parameter	0.0
$\chi_1$	maximum substrate affinity parameter	5.0
$\delta_b$	interphase repulsion parameter	0.05
$\theta_{e0}$	critical ECM threshold	$[0, 1]$
Mass transfer parameters		
$\theta_{n1}$	lower cell volume fraction threshold	0.4
$\theta_{n2}$	upper cell volume fraction threshold	0.6
$k_m^n$	rate of mitosis	0.8
$k_m^d$	rate of apoptosis	0.1
$k_m^s$	rate of ECM deposition	0.05

#### 3.1 PLLA scaffold heterogeneity

To illustrate the model behaviour, in Figure 4 we present simulations corresponding to the case for which cells are seeded within a PLLA scaffold of uniform porosity and their interactions with the PLLA scaffold and deposited

ECM are identical; that is, we employ Equation (16a) to initialise  $\theta_s$  and choose  $\chi = \text{constant}$  in place of (11). Figure 5 shows corresponding simulation results in the case for which  $\theta_s(x, 0)$  is specified via Equation (16b).

Figures 4(a) and (b) reveal that the cells proliferate and deposit ECM asymmetrically under the influence of perfusion. The PLLA scaffold degrades uniformly so that  $\theta_s = \theta_s(t)$  in  $a \leq x \leq b$ . Near  $x = a, b$  where the cell volume fraction is small, PLLA degradation dominates ECM deposition and a decrease in total substrate fraction is observed; in regions of high cell volume fraction, ECM deposition ensures that the substrate density is maintained or increased. Figure 4(a) indicates that the cell volume fraction tends to a spatially-uniform value  $\theta_n = \theta_{n_2}$ . As  $\theta_n$  reaches  $\theta_{n_2}$ , the transition to the apoptotic phenotype precludes any further increase in cell density. Re-entry to the proliferative phenotype on subsequent reduction of cell density ensures a uniform distribution is maintained; the ECM deposition is greatest upstream due to perfusion causing advection of cells downstream, so that  $\theta_n$  attains the upper threshold at later times.

Figure 4 indicates that, when compared to the spatially uniform case (see Figures 4–7 of O'Dea et al (2010)) in the regime shown, the addition of spatial variation to the substrate phase via ECM deposition does not affect significantly the dynamics of the other model variables shown in Figures 4(d)–(f). This behaviour has been discussed in our previous work (O'Dea et al, 2010). Here, it suffices to note that the interplay between aggregative and repulsive cell behaviour (see Equation (10)) is reflected in the evolution of the pressures and velocities of each phase (see Figures 4(d)–(f); the cell phase pressure is omitted for brevity). At low cell volume fraction (early times), aggregation dominates and the cell phase velocity indicates cell movement towards the centre of the population to form a dense aggregate; at high cell volume fraction (later times) repulsive effects dominate, leading to migration away from the central region; aggregative effects dominate at the edges of the population where the cell population remains low. Combined, these effects generate a dense cell aggregate, with steep spatial gradients of cell volume fraction near its up- and down-stream periphery (shown by the final line in Figure 4(a)). To conserve mass, the culture medium phase moves in the opposite direction.

Comparison of Figures 4 and 5 shows that, while the global features of the predicted cell and ECM volume fractions remain similar, the introduction of PLLA scaffold heterogeneity induces short-range variations in cell and ECM volume fractions and, additionally, has a dramatic influence on the cells' fluid-mechanical environment, with significant variations in culture medium velocity evident over the short lengthscale associated with the heterogeneity of the substrate (Figure 5(e)).

The importance of the scaffold (and ECM) distribution on the culture medium and cell phase velocities is evident from Equation (5), which shows that spatial gradients in  $\Theta = \theta_s + \theta_e$  influence the culture medium pressure gradient, leading to significant changes in culture medium flow. In addition, the axial cell phase velocity, obtained by integrating the axial component of the cell phase momentum equation (Equation (22), Appendix A, in the long-wavelength limit), is defined as follows:

$$u_n = \frac{1}{12\mu_n} \left( -\frac{\partial p_w}{\partial x} + \frac{\partial \Theta}{\partial x} \frac{p_w}{\theta_n} - \frac{1}{\theta_n} \frac{\partial}{\partial x} \left( \theta_n^2 \Sigma \right) - \frac{\partial}{\partial x} (\Theta \psi) \right), \quad (18)$$

which indicates that, under the influence of the second and final terms, the large variations in substrate porosity present in Figures 2 and 5(b) will lead to significant changes in cell velocity. (We also note that the singularity in  $\theta_s$  at  $x = a, b$  therefore leads to the spike in cell and culture medium velocities, illustrated in Figures 4(e,f) and 5(e,f).) Additionally, inspection of Equations (10) and (18) reveals that active movement of cells within the tissue construct (embodied in the final two terms of (18)) results from a balance between aggregation, attachment to the substrate and repulsion, regulated by  $\chi$ ,  $\nu$ ,  $\delta_a$  and  $\delta_b$ . Spatial gradients of the cell and substrate phases also influence this behaviour: when  $\nu$  and  $\chi$  are constant, aggregation and attachment modify the cells' velocity via:

$$\frac{1}{6\mu_n} \left( \nu \frac{\partial \theta_n}{\partial x} + \frac{\chi}{2} \frac{\partial \Theta}{\partial x} \right), \quad (19)$$

so that when aggregation or attachment dominates repulsion, cells move up spatial gradients of  $\theta_n$  and  $\Theta$ ; in view of Equations (5), (10) and (18), spatial gradients of  $\Theta$  additionally modulate cell advection via the culture medium pressure. Given the importance of culture medium flow-induced mechanical stimulation to the growth and differentiation of various cell types (see §1 and §2.3), such variations in cell and culture medium velocity are likely to have a significant effect on local cell behaviour.

We pause to remark that Figures 4(a) and 5(a) show that as the cell population expands to colonise the scaffold, our fluid-based model allows egress of cells (and, eventually, the subsequently deposited ECM) from the scaffold into the up- and downstream regions ( $x < a$  and  $x > b$ ). Lemon and King (2007) demonstrate that, due to cell-scaffold adhesion, such behaviour is minimised in scaffolds whose density distributions decay to zero at the boundaries; we have, however, employed experimentally-relevant data to initialise  $\theta_s$  here. Cell egress is not

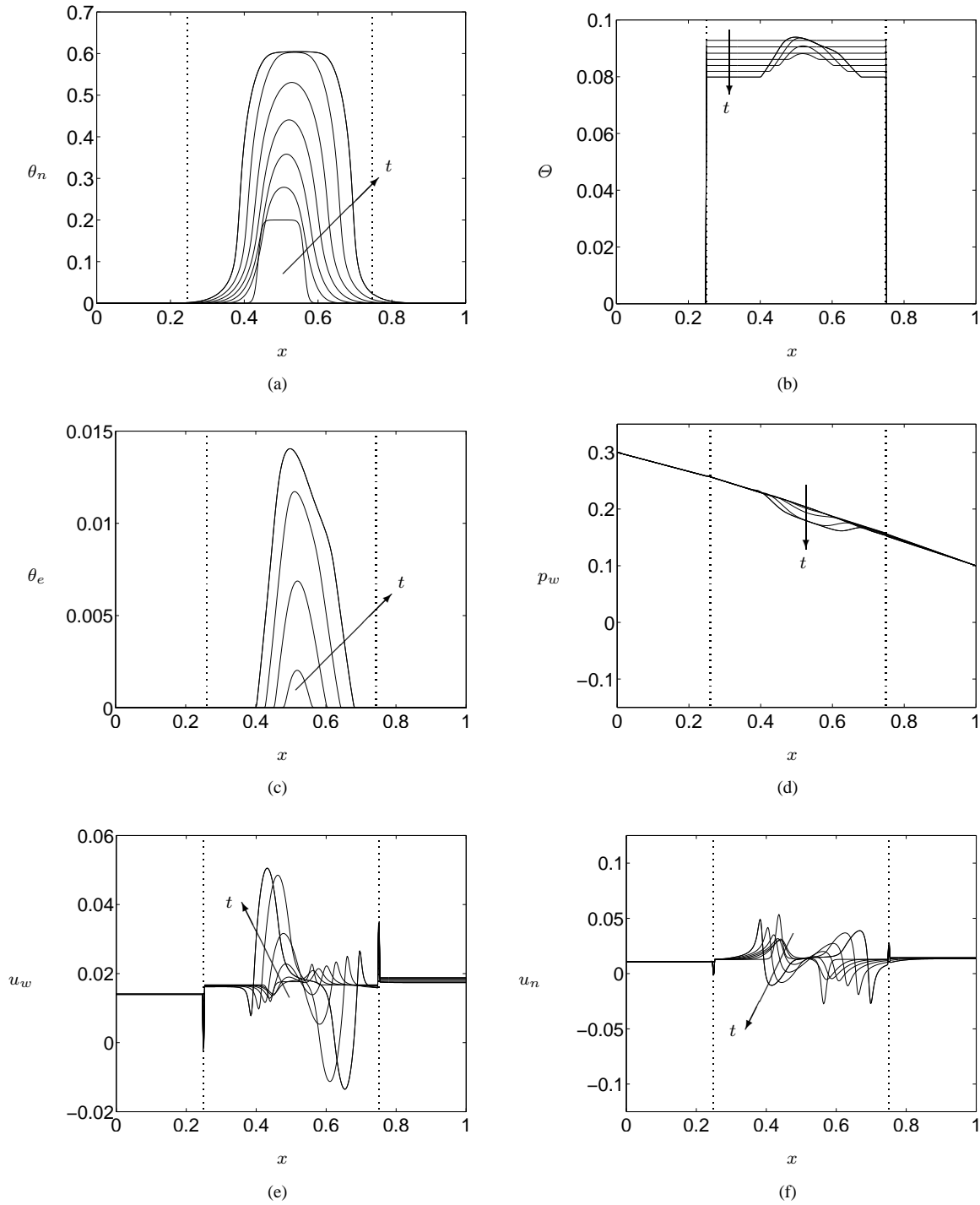


**Fig. 4** Illustrative plots of the evolution of (a) the cell volume fraction ( $\theta_n$ ), (b) the substrate volume fraction ( $\Theta$ ), (c) the ECM volume fraction ( $\theta_e$ ), (d) the culture medium pressure ( $p_w$ ), (e) the axial culture medium velocity ( $u_w$ ), and (f) the axial cell phase velocity ( $u_n$ ) in the regime of cell volume fraction-dependent cell proliferation and ECM deposition, uniform scaffold degradation, and uniform cell-scaffold interaction properties at times  $t = 0 - 3$  (in steps of  $t=0.5$ ). The model parameters are as described in Table 1 except  $\chi = \chi_1$  in place of (11). Initial conditions are given by (15), (16a) and (17). Vertical dotted lines indicate the end points of the scaffold at  $x = a, b$ .

desirable in the current context of a perfusion bioreactor (and is in any case minimal in the seeding protocol employed here: the cell flux  $\theta_n u_n$  is small); however, it is of biological relevance to modelling tissue invasion after implantation.

### 3.2 Cell-substrate interactions

In this subsection we investigate the influence of the properties of PLLA scaffold on the eventual construct composition, both in terms of its spatial distribution and its interactions with the cells.

First, we compare simulation results for which  $\chi = \text{constant}$  with those for which cell-scaffold adherence is governed by (11) and, in so doing, investigate how a disparity between cell-scaffold and cell-ECM attachment strength (due to the surface chemistry of the polymer scaffold) may influence the composition of the developing construct. For clarity, we employ Equation (16a) to initialise  $\theta_s$ , corresponding to a PLLA scaffold of initially uniform porosity; the combined influence of cell-substrate interactions and scaffold heterogeneity on construct composition is investigated subsequently.

In Figures 6(a) and (b), we assume that the cells' affinities for the PLLA scaffold and the deposited ECM are identical; the figures show cell and scaffold phase distributions at illustrative time points for different values of  $\chi$ . Comparison of the construct composition when  $\chi = 0$  and  $\chi = 5$ , suggests that cell migration up spatial gradients of  $\Theta$  leads to a more sharply-defined cell volume fraction profile; however, the maximal volume fraction is reduced.

Inspection of the cell volume fraction distribution at later times reveals more interesting behaviour. As  $\theta_n$  increases, advection of cells becomes more significant, leading to profiles which are skewed in the downstream direction. For large cell volume fraction, the combination of advection and cell-cell and cell-substrate repulsion leads to cell migration away from the aggregate's centre. This outward drift is balanced by inward movement of cells at the periphery of the densely populated region. In the case of strongly adherent cells, increased (inward) movement up spatial gradients of  $\Theta$  causes the cell volume fraction to peak at the periphery of the aggregate, with a flatter profile near the centre (see the final profile in Figure 6(a) in the case  $\chi = 5$ ). For small values of  $\chi$ , a profile similar to that shown in Figure 4(a) is obtained.

Figures 6(c) and (d) show how the construct composition is influenced by differential adhesion between the porous scaffold and the deposited ECM. The cells' adherent behaviour is modelled by Equation (11) so that  $\chi$  varies between  $\chi_0 = 0$  and  $\chi_1 = 5$  in response to the ECM volume fraction; we present results for a series of different values  $\theta_{e0} = -1, 0 - 0.025, 1$  which dictate the threshold value at which the cells affinity for the substrate is altered due to ECM presence. The choices  $\theta_{e0} = -1$  and  $\theta_{e0} = 1$  correspond to  $\chi = 5$  and  $\chi = 0$ , since the threshold is intentionally set outside the range of  $\theta_e$  observed in simulation; the values  $\theta_{e0} = 0 - 0.025$  are chosen to span the observed range.

Comparison of Figures 6(a,b) and 6(c,d) indicate that in the case of a uniform initial scaffold, preferential adherence to ECM leads to the creation of a tissue construct whose composition is indistinguishable from that obtained when the adherence properties of the substrate are uniform. Corresponding results were obtained when the initial scaffold porosity was spatially-nonuniform, but are not included. The influence of changing the threshold  $\theta_{e0}$  is therefore restricted to altering the 'average' value of the cell-scaffold affinity parameter  $\chi$ ; its local value due to changes in ECM volume fraction does not affect significantly the cell density. In view of this somewhat surprising outcome, we conclude that the mathematical complexity associated with the biologically-inspired cell-substrate interactions (and embodied by Equation (11)) adds no additional predictive capability to the model. Henceforth, we return to the simplified model in which  $\chi = \text{constant}$ . We note that in this case, inspection of Equations (5) and (10) reveals that the influence of the cell-scaffold affinity strength on the model behaviour may only be studied in the presence of a spatially-heterogeneous substrate volume fraction, since it appears in the combination  $\chi \frac{\partial}{\partial x} (\theta_n \frac{\partial \Theta}{\partial x})$ ; our previous work (O'Dea et al, 2010), which assumed  $\Theta = \text{constant}$  therefore neglected its influence.

In Figure 7 we demonstrate how the combined effects of cell-substrate interactions ( $\chi = \text{constant}$ ) and the heterogeneity of PLLA scaffold volume fraction influences the construct composition. As indicated by Equation (18), strong cell-scaffold adherence enhances cell movement up scaffold and ECM gradients. Large, short-range spatial gradients of scaffold porosity exist in the experimental data we have employed to initialise  $\theta_s$ . We therefore observe large deviations in cell and ECM distributions, which mirror, and exaggerate, the underlying PLLA scaffold porosity distribution. Since the deposition of ECM (and other associated extracellular materials) enables the maintenance of the mechanical properties of the degrading PLLA scaffold, such heterogeneous ECM distributions have important implications regarding the structural suitability and suitability for implant of the resulting construct. With this in mind, in the following subsection we focus on the interplay between PLLA degradation and ECM deposition and the maintenance of substrate porosity during this process.

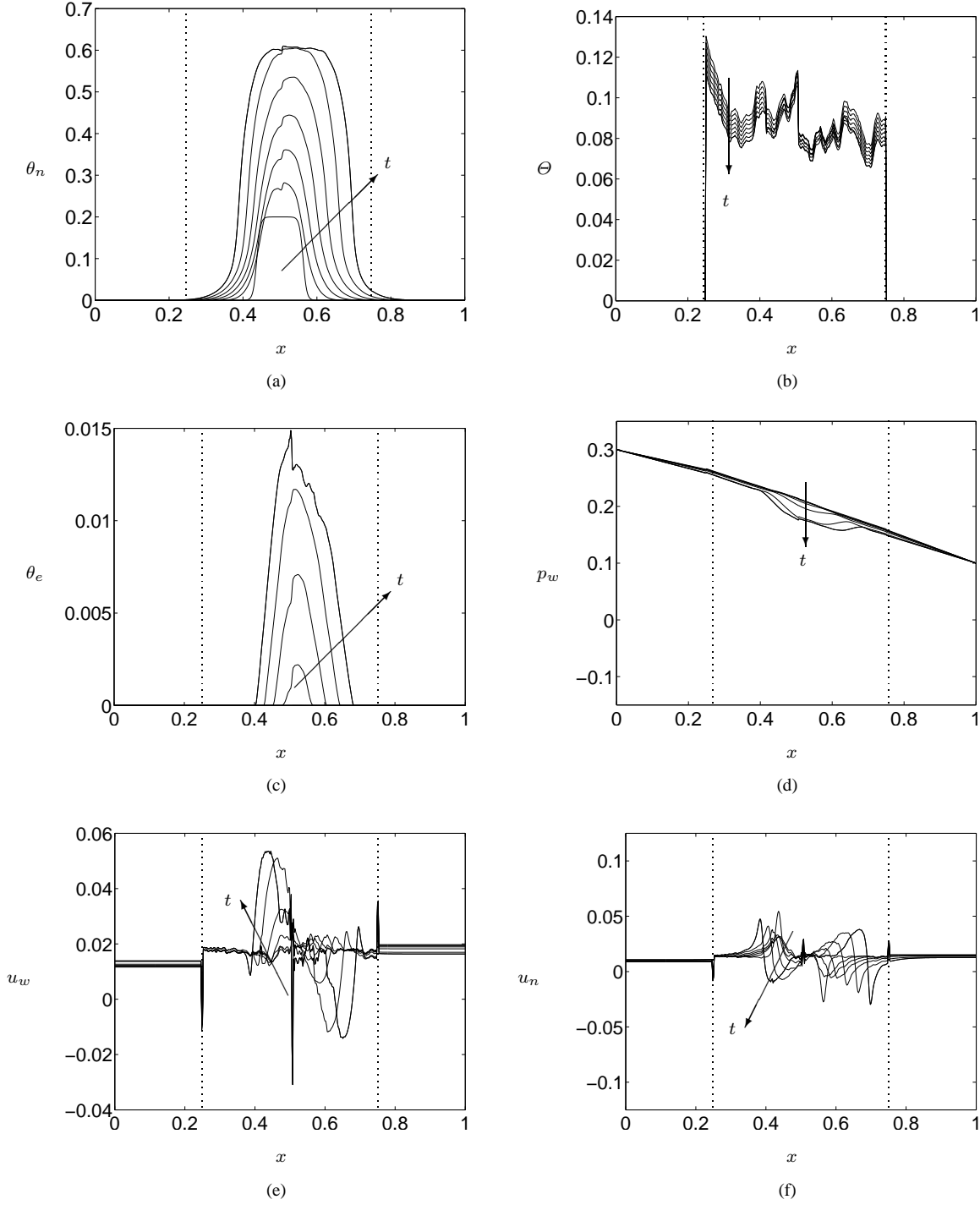


**Fig. 5** Results from a typical simulation showing the evolution of (a) the cell volume fraction ( $\theta_n$ ), (b) the substrate volume fraction ( $\Theta$ ), (c) the ECM volume fraction ( $\theta_e$ ), (d) the culture medium pressure ( $p_w$ ), (e) the axial culture medium velocity ( $u_w$ ), and (f) the axial cell phase velocity ( $u_n$ ) in the regime of cell volume fraction-dependent cell proliferation and ECM deposition, uniform scaffold degradation, and uniform cell-scaffold interaction properties at times  $t = 0 - 3$  (in steps of  $t=0.5$ ). Parameters values: as in Table 1, except  $\chi = \chi_1$  in place of (11). Initial conditions are given by (15), (16b) and (17). Vertical dotted lines indicate the end points of the scaffold at  $x = a, b$ .

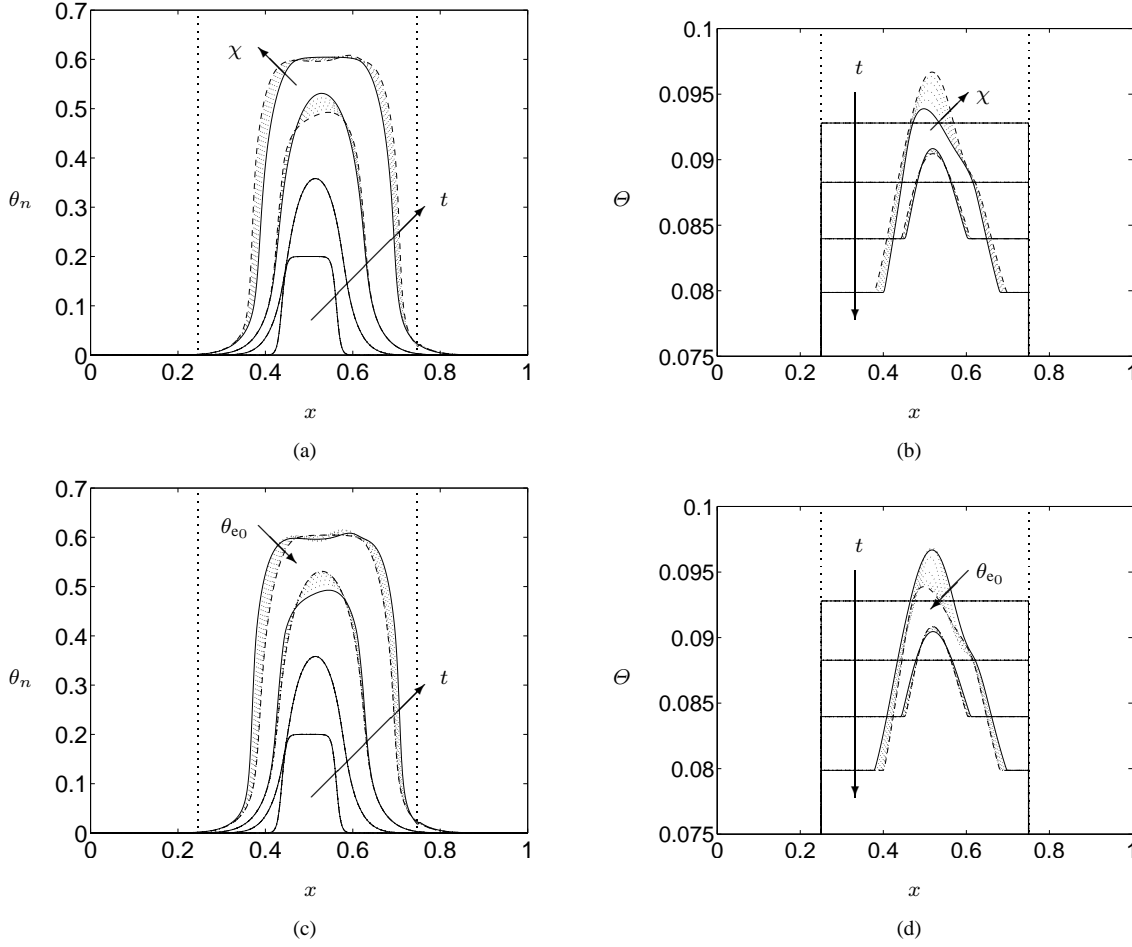


**Fig. 6** The evolution of the construct composition (at times  $t = 0, 1, 2, 3$ ) in the regime of cell density dependent growth and degradation; arrows indicate the direction of increasing time. In (a) and (b) the predicted cell and substrate volume fractions are shown for various values of cell-substrate interaction parameter values:  $\chi = 0 - 5$  (in steps of  $\chi = 1$ ),  $\delta_b = 0.05$ ; the arrows indicate the direction of increasing  $\chi$ . In (c) and (d), the cell and substrate volume fractions are depicted in the case for which cell-substrate interactions are governed by (11) for  $\theta_{e0} = -1$  ( $\chi = 5$ ; solid line),  $\theta_{e0} = 0 - 0.025$  in steps of  $\theta_{e0} = 0.005$  (dotted lines) and  $\theta_{e0} = 1$  ( $\chi = 0$ ; dashed line). The arrows indicate the direction of increasing  $\theta_{e0}$ . Initial conditions are given by (15), (16a) and (17). Except as stated, all parameters are as given in Table 1. Vertical dotted lines indicate the scaffold periphery at  $x = a$  and  $x = b$ .

### 3.3 Scaffold degradation

The maintenance of tissue construct mechanical properties is crucially affected by achieving a match between the rates of scaffold degradation and deposition of ECM and other extracellular materials. In this section we indicate how our model may be employed to determine how the evolution of the substrate volume fraction depends on the model parameters. For clarity, in preference to the spatio-temporal distributions presented in §§3.1,3.2, we consider the evolution of the total substrate volume  $\bar{\Theta}(t)$ , and its PLLA and ECM components  $\bar{\theta}_s(t)$ ,  $\bar{\theta}_e(t)$ , which are defined as follows:

$$\bar{\Theta}(t) = \bar{\theta}_s(t) + \bar{\theta}_e(t); \quad \bar{\theta}_s(t) = \int_0^1 \theta_s(x, t) dx, \quad \bar{\theta}_e(t) = \int_0^1 \theta_e(x, t) dx. \quad (20)$$

The simulations presented in Figure 8 demonstrate that close control of scaffold degradation and ECM deposition is required in order to maintain substrate density. We do not present the corresponding cell volume fraction evolution since our focus here is on the tissue construct's rigid, load-bearing components. In Figure 8(a), we consider a non-degrading scaffold, and the evolution of the substrate volume fraction is therefore determined by the evolution of the ECM phase. With the addition of scaffold degradation (Figure 8(b)), we observe an initial decrease in substrate due to scaffold degradation; as the seeded cell population increases, Equation (14) leads to progression



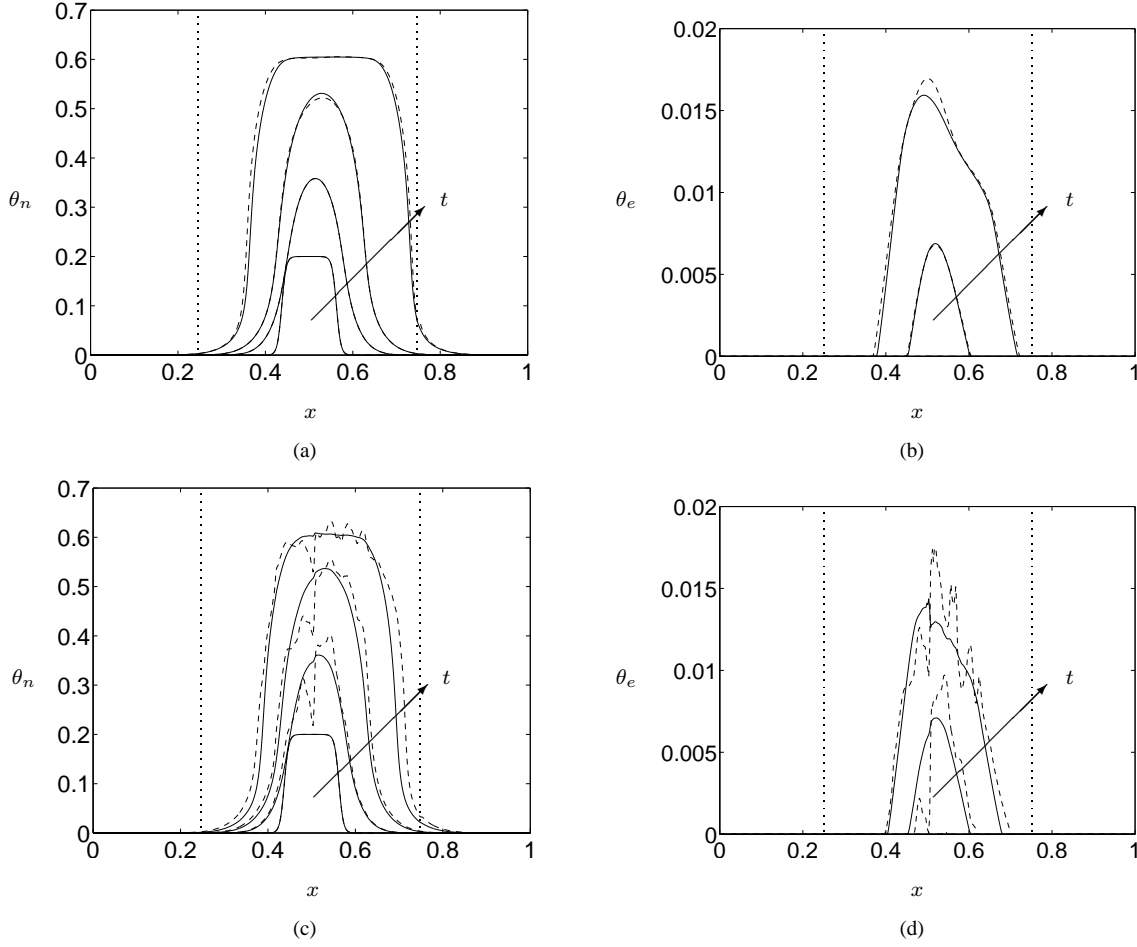


**Fig. 7** The evolution of the cell volume fraction ( $t = 0, 1, 2, 3$ ) and the ECM volume fraction ( $t = 2, 3$ ) in the case of cell volume fraction dependent cell proliferation and ECM deposition defined by Equations (12) and (14); arrows indicate the direction of increasing time. Plots are for  $\chi = 1$  (solid line) and  $\chi = 0$  (dashed line). In (a), (b) Initial conditions are given by (15), (16a) and (17) and in (c), (d) Equation (16b) is employed to specify  $\theta_s(x, 0)$ . Except as stated, all parameters are as given in Table 1. Vertical dotted lines indicate the end points of the scaffold at  $x = a, b$ .

to an ECM-depositing phenotype and the substrate volume fraction increases. Our model predicts that, eventually, the cell volume fraction will increase to a point at which all cells in the scaffold enter apoptosis, at which point the substrate volume fraction achieves an equilibrium level. However, the timescale over which we perform our simulations is restricted by our wish to restrict tissue egress from the scaffold into the up- and downstream regions  $x < a, x > b$  (see §3) and we therefore do not observe such equilibrium behaviour. Nevertheless, our simulation results indicate that the rate of scaffold degradation is a key experimental variable, and suggest that there is a threshold time, before which the construct's mechanical properties are likely to be unsuitable for implantation.

#### 4 Discussion

In this paper we have presented a multiphase model describing tissue growth within a perfusion bioreactor, modelled as a two-dimensional channel containing cells, culture medium, a porous PLLA scaffold and deposited ECM. The formulation employed is based on the general multiphase formulation proposed in Lemon et al (2006) and extends the three phase model of O'Dea et al (2010), where the PLLA scaffold was assumed to be spatially-homogeneous and inert. Many similar studies of tissue growth have employed this simplifying assumption, tacitly assuming that the importance of spatial variation of scaffold/ECM volume fraction is negligible. Here, we include additional mass conservation equations for the scaffold and ECM phases with which to model scaffold degradation and ECM deposition. This allows us to incorporate PLLA scaffold phase heterogeneity, inhomogeneous deposition

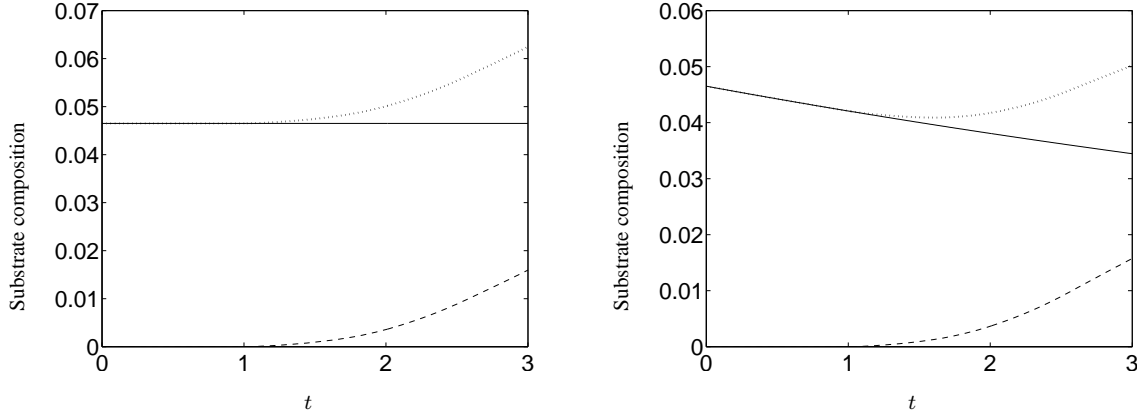


**Fig. 8** The evolution of the volume fraction of: the substrate,  $\bar{\theta}$  (dotted line); the ECM,  $\bar{\theta}_e$  (dashed line); and the PLLA scaffold,  $\bar{\theta}_s$  (solid line), over time for two different values of the PLLA scaffold degradation rate,  $k_d^s$ . In (a)  $k_d^s = 0.0$ , (b)  $k_d^s = 0.1$ . An increased ECM deposition rate of  $k_m^e = 0.1$  is used to amplify the deposition of ECM. Initial conditions are given by (15), (16b) and (17). Except as stated, all parameters are as given in Table 1.

of ECM, and to consider explicitly the interactions between cells and their different supporting structures, while remaining within a simplified modelling framework.

Comparison of our simulation results with our previous work (O'Dea et al, 2010) indicates that the predicted cell volume fraction and variables related to the mechanical environment are strongly affected by heterogeneous scaffold volume fraction distributions; for instance, the culture medium velocity shows strong short-range variation, which is likely to have a profound effect on the mechanical environment of the cells. Additionally, we have demonstrated that ECM deposition by the cells is highly localised in the regions of elevated cell volume fraction and that spatial variation in the PLLA scaffold volume fraction leads to large deviations in cell and ECM distributions.

In addition to spatial variation of the scaffold volume fraction, and motivated by the possible variation in cell binding sites in tissue engineering scaffolds, we considered the heterogeneous interactions between cells and their supporting scaffold and the deposited ECM, postulating that cells have a greater affinity for ECM (and other deposited materials) than the scaffold onto which they are deposited. Employing a smoothed switch between low and high affinity in response to the local ECM volume fraction, we showed that such a disparity has no significant influence on eventual construct composition. This conclusion indicates that simplified models in which cells interact uniformly with their supporting structures may be employed without affecting their biological relevance (in the present study, this corresponds to  $\chi = \text{constant}$ ). We showed that in such a simplified model cell-scaffold/ECM interactions can have dramatic effects on the construct composition, leading to significantly enhanced migration of cells up spatial gradients of substrate volume fraction. In the case of experimentally-relevant initial PLLA scaffold porosity distributions, which display large gradients in scaffold distribution, this leads to cells and ECM profiles which mirror and exaggerate the underlying scaffold porosity. The heterogeneity of the resulting tissue construct has important ramifications for its structural stability and suitability for implant.

While we treat the construct's load-bearing components as rigid porous material for simplicity, and therefore do not model its mechanical properties (such as yield stress, or elasticity), we nevertheless employ our model to draw conclusions regarding the suitability of constructs for implantation from a mechanical perspective as follows. Our model associates scaffold degradation with a reduction in scaffold phase volume fraction, from which we infer deleterious effects on the construct's mechanical properties, which are ameliorated by deposition of ECM (and other extracellular materials). Under such an assumption, it is clear that the interplay between scaffold degradation and ECM deposition is crucial in maintaining the construct's mechanical properties, thereby avoiding failure of implants under *in vivo* conditions. The results of our simulations discussed above indicate that the production of scaffolds with uniform porosity may play an important role in producing tissue constructs with mechanical properties appropriate for implant. Furthermore, we highlight that the rate of scaffold degradation is a key experimental variable, and that there may be a threshold time, before which the construct's mechanical properties are likely to be unsuitable for implantation.

We have extended our previous studies (O'Dea et al, 2008, 2010; Osborne et al, 2010), by accommodating spatial non-uniformity in scaffold and ECM volume fraction, demonstrating the importance of such a consideration; however, we have made a number of simplifying assumptions to enable analysis. We have restricted attention

to a rigid scaffold and ECM phase (the remaining phases being modelled as viscous fluids) and so our formulation applies to those constructs whose solid characteristics are dominated by the rigidity of the scaffold and/or deposited materials. We note also that our simplified treatment of the PLLA scaffold and ECM means that the mechanics of our model are in fact accommodated within a three phase framework. Our model formulation is further simplified by exploiting the long-wavelength limit; our previous work (Osborne et al, 2010) has indicated that, while two-dimensional variation of mechanical stimulation has an important effect on construct growth, the long-wavelength limit provides a good approximation to the averaged behaviour of the two-dimensional model, even for bioreactors with large aspect ratio. Nevertheless, validation of our model results within a two-dimensional framework remains important future work. We have assumed that the scaffold degrades uniformly; however, it is known that bi-products of tissue growth can influence the mechanical and structural nature of tissue engineering scaffolds (see, *e.g.*, Ahearne et al (2010) and references therein). Consideration of such effects represents another interesting extension to our study.

We have employed our simplified formulation to make inferences regarding the likely composition and mechanical integrity of engineered tissue constructs. Important further work includes explicit modelling of the mechanical properties of the scaffold and ECM, considering, for example, a poroelastic (Roose et al, 2003) or poroviscoelastic (Byrne and Preziosi, 2003) model. Additionally, the robustness of our conclusions should be investigated by considering the addition of nutrient-limited growth to our formulation; methodologies for such investigations are given by Lewis et al (2005) and Lemon and King (2007). Such a sophisticated model will allow for validation against histological samples from relevant experimental studies.

## 5 Acknowledgements

This work was supported by funding from the EPSRC in the form of a Ph.D studentship (RDO) and an Advanced Research Fellowship (SLW). It was also supported by the EPSRC/BBSRC-funded OCISB project BB/D020190/1 (JMO), and based on work supported in part by Award KUK-013-04 (HMB) made by King Abdullah University of Science and Technology (KAUST). We are also grateful to E. Baas, ISTM, Keele University for the provision of experimental data.

## A Model derivation

We consider a bioreactor of length  $L^*$  and width  $h^*$ , modelled as a two-dimensional channel containing a mixture of four interacting phases, representing cells, culture medium, PLLA scaffold and ECM. The viscosity of each phase is denoted  $\mu_i^*$  (where  $i = n, w, s, e$  indicates variables associated with the cell, culture medium, scaffold and ECM phases, respectively), and the typical timescale for tissue growth (comprising both cell proliferation and ECM deposition) is denoted  $K^*$ . Asterisks distinguish dimensional quantities from their dimensionless equivalents.

We introduce a Cartesian coordinate system  $L^*x = L^*(x, y)$  and time  $K^*t$  and the channel occupies the dimensionless region  $0 \leq x \leq 1, 0 \leq y \leq h = h^*/L^*$ . The volume fraction of each phase is denoted  $\theta_i$ , while the dimensionless volume-averaged velocities, pressures and stress tensors of the each phase are denoted  $K^*L^*u_i = K^*L^*(u_i, v_i)$ ,  $K^*\mu_w^*p_i$  and  $K^*\mu_w^*\sigma^i$ . Tissue growth, scaffold degradation and ECM deposition are captured via material transfer functions  $K^*S_i$ . We assume that all dimensionless dependent variables are functions of  $x$  and  $t$ .

The model is constructed by considering mass and momentum balances for each phase, assuming that each phase is incompressible, with equal density, and neglecting inertial effects; the equations governing the  $i^{\text{th}}$  phase (with volume fraction  $\theta_i$ ) are as follows (see Lemon et al (2006); O'Dea et al (2010); Osborne et al (2010)):

$$\frac{\partial \theta_i}{\partial t} + \nabla \cdot (\theta_i \mathbf{u}_i) = S_i(\theta_k, p_k, \mathbf{u}_k), \quad (21)$$

$$\nabla \cdot (\theta_i \sigma^i) + \sum_{j \neq i} \mathbf{F}^{ij} = \mathbf{0}. \quad (22)$$

Additional conservation conditions may be obtained by summing over all phases and exploiting the no-voids condition  $\sum_i \theta_i = 1$ .

In Equation (21)  $K^*S_i$  is the net material production term associated with phase  $i$  (mass conservation demands that  $\sum S_i = 0$ ); in (22),  $K^*\mu_w^*/L^*\mathbf{F}^{ij}$  is the interphase force exerted by phase  $j$  on phase  $i$ , obeying  $\mathbf{F}^{ij} = -\mathbf{F}^{ji}$ . These interphase forces comprise interphase viscous drag (with drag coefficient  $\mu_w^*/L^*k$ ) and active forces, the latter being embodied within extra pressures which arise due to cell-cell, cell-ECM and cell-scaffold interactions; interactions between the culture medium and scaffold phases are assumed to involve only viscous drag. The mechanics of this four phase formulation is simplified by lumping the scaffold and ECM components into a single 'substrate' phase, denoted  $\theta_S = \theta_s + \theta_e$ , and modelled as a rigid porous material. For notational convenience, in this Appendix, we employ the subscript  $S$  to denote the substrate, in preference to  $\Theta$ . Separate mass conservation equations are nevertheless employed for  $\theta_s$  and  $\theta_e$  to track their individual evolution.

The cell population and culture medium are represented as distinct viscous fluids, modelled by standard viscous stress tensors; for consistency we choose the same form for  $\sigma^S$ , taking the limit  $\mu_S^* \rightarrow \infty$ ,  $\mathbf{u}_S \rightarrow 0$ . These constitutive assumptions are embodied in the following equations.

$$\sigma^i = -p_i \mathbf{I} + \mu_i \left( \nabla \mathbf{u}_i + \nabla \mathbf{u}_i^T \right) - \frac{2}{3} (\nabla \cdot \mathbf{u}_i) \mathbf{I}, \quad \text{for } i = n, w, \quad (23)$$

$$\mathbf{F}^{ij} = (p_w + \psi_{ij}) (\theta_j \nabla \theta_i - \theta_i \nabla \theta_j) + k \theta_i \theta_j (\mathbf{u}_j - \mathbf{u}_i), \quad \text{for } i, j = n, w, S, \quad (24)$$

$$p_n = p_w + \Sigma_n + \theta_n \psi_{nS}, \quad (25)$$

wherein  $\mu_i$  are the dimensionless viscosities of each phase, and  $\Sigma_n$  and  $\psi_{nS}$  are defined

$$\Sigma_n = -\theta_n \nu + \frac{\delta_a \theta_n^2}{\theta_w} \quad \text{and} \quad \psi_{nS} = -\chi + \frac{\delta_b \theta_n}{\theta_w}. \quad (26)$$

In Equation (26)  $\nu$ ,  $\chi$ ,  $\delta_a$ ,  $\delta_b > 0$  dictate the cells' tendency to aggregate, their affinity for the scaffold/ECM and the strength of cell-cell/cell-scaffold repulsion. Full details of the above choice of interphase interaction terms may be found in Lemon *et al* (2006).

Figure 9 depicts the two-dimensional model of the bioreactor, together with appropriate boundary conditions. These correspond to no-slip and no-penetration of cells or culture medium through the channel walls, a pressure-driven flow imposed via up- and downstream pressures  $K^* \mu_w^* P_U$  and  $K^* \mu_w^* P_D$ , partitioned normal stress conditions and fully-developed flow at  $x = 0, 1$ .

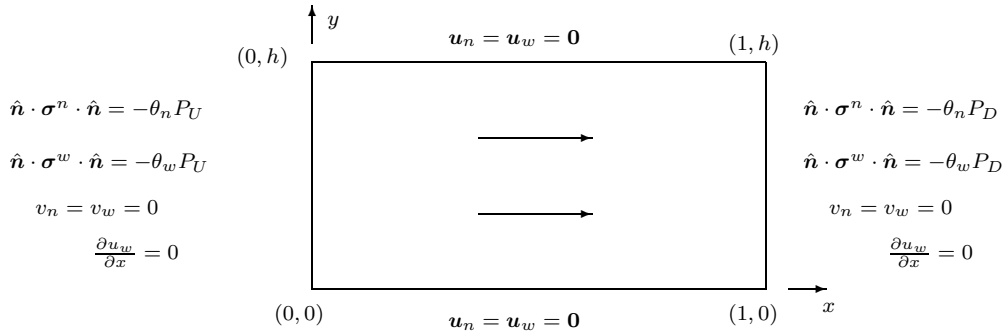


**Fig. 9** The two-dimensional domain, outward-pointing normal  $\hat{\mathbf{n}}$  and associated boundary conditions. The arrows indicate the perfusion direction in the case of dimensionless up- and downstream pressures  $P_U$  and  $P_D$  obeying  $P_U > P_D$ .

We now simplify the two-dimensional equations by considering the limit for which the aspect ratio of the bioreactor is asymptotically small ( $h \ll 1$ ). We remark that, since the culture medium volume fraction may be eliminated via  $\theta_w = 1 - \theta_n - \theta_s - \theta_e$  and the substrate is rigid, we need consider momentum conservation equations for the fluid (cell and culture medium) phases, only.

Following O'Dea *et al* (2010), the reduced model is obtained by rescaling according to:

$$y = h\bar{y}, \quad v_i = h\bar{v}_i, \quad p_i = \bar{p}_i/h^2, \quad (27)$$

and averaging across the channel in the transverse direction (imposing the boundary conditions at  $y = 0, h$  depicted in Figure 9). We find that the pressure and the volume fraction of each phase are functions of  $x$  and  $t$  only and the flow of cells and culture medium is unidirectional at leading order ( $\bar{v}_i = 0$ ). Expressions for the averaged axial velocities  $\langle \bar{u}_w \rangle$  and  $\langle \bar{u}_n \rangle$  are obtained from the remaining momentum equations, on substitution of which into the (averaged) mass conservation equations (dropping the overbars), we obtain the following system of coupled partial differential equations for the volume fractions  $\theta_e(x, t)$ ,  $\theta_s(x, t)$ ,  $\theta_n(x, t)$  and the culture medium pressure,  $p_w(x, t)$ :

$$\frac{\partial \theta_e}{\partial t} = S_e, \quad (28)$$

$$\frac{\partial \theta_s}{\partial t} = S_s, \quad (29)$$

$$\frac{\partial \theta_n}{\partial t} + \frac{1}{12\mu_n} \frac{\partial}{\partial x} \left( \theta_n \frac{\partial p_w}{\partial x} \right) = S_n, \quad (30)$$

$$\begin{aligned} \frac{\partial}{\partial x} \left\{ (\theta_n + \mu_n(1 - \theta_s - \theta_e - \theta_n)) \frac{\partial p_w}{\partial x} - p_w \frac{\partial}{\partial x} (\theta_e + \theta_s) \right\} \\ + \frac{\partial}{\partial x} \left\{ \frac{\partial(\theta_n \Sigma_n)}{\partial x} + \theta_n \frac{\partial((\theta_e + \theta_s) \psi_{nS})}{\partial x} \right\} = 0, \end{aligned} \quad (31)$$

in which  $\mu_n$  is the relative viscosity of the cell and culture medium phases. The extra pressures  $\Sigma_n$  and  $\psi_{nS}$  are scaled according to equation (27) so that these interactions are retained at leading order, which implies  $(\nu, \delta_a, \chi, \delta_b) = (\bar{\nu}, \bar{\delta}_a, \bar{\chi}, \bar{\delta}_b)/h^2$ ; the remaining

parameters are  $\mathcal{O}(1)$ . Equations (28)–(31) embody conservation of mass for the ECM, PLLA scaffold and cell phases, and the multiphase mixture.

Under the rescaling, (27), the boundary conditions shown in Figure 9 become:

$$p_w = P_U \quad \text{at } x = 0, \quad (32)$$

$$p_w = P_D \quad \text{at } x = 1, \quad (33)$$

$$\frac{\partial \theta_n}{\partial x} = 0 \quad \text{at } x = 0, 1. \quad (34)$$

## References

- Adachi T, Osako Y, Tanaka M, Hojo M, Hollister S (2006) Framework for optimal design of porous scaffold microstructure by computational simulation of bone regeneration. *Biomater* 27:3964–3972
- Ahearne M, Wilson S, Liu KK, Rauz S, El Haj A, Yang Y (2010) Influence of cell and collagen concentration on the cell-matrix mechanical relationship in a corneal stroma wound healing model. *Exp Eye Res* 91:584–591
- Araujo R, McElwain D (2005) A mixture theory for the genesis of residual stresses in growing tissues i: A general formulation. *SIAM J of Appl Math* 65(4):1261–1284
- Bakker A, Klein-Nulend J, Burger E (2004a) Shear stress inhibits while disuse promotes osteocyte apoptosis. *Biochem Biophys Res Commun* 320(4):1163–1168
- Bakker A, Klein-Nulend J, Burger E (2004b) Shear stress inhibits while disuse promotes osteocyte apoptosis. *Biochem Biophys Res Commun* 320:1163–1168
- Breward C, Byrne H, Lewis C (2002) The role of cell-cell interactions in a two-phase model for avascular tumour growth. *J Math Biol* 45:125–152
- Burdick J, Mauck R (eds) (2010) *Biomaterials for Tissue Engineering Applications: A Review of the Past and Future Trends*. Springer, Wien
- Byrne D, Lacroix D, Planell J, Kelly D, Prendergast P (2007) Simulation of tissue differentiation in a scaffold as a function of porosity, Young's modulus and dissolution rate: application of mechanobiological models in tissue engineering. *Biomater* 28(36):5544–5554
- Byrne H, Preziosi L (2003) Modelling solid tumour growth using the theory of mixtures. *Math Med Biol* 20(4):341–366
- Cartmell S, El Haj A (2005) Mechanical bioreactors for tissue engineering. In: Chaudhuri J, Al-Rubeai M (eds) *Bioreactors for tissue engineering: Principles, Design and Operation*, Springer, Dordrecht, The Netherlands, chap 8, pp 193–209
- Chaplain M, Graziano L, Preziosi L (2006) Mathematical modelling of the loss of tissue compression responsiveness and its role in solid tumour development. *Math Med Biol* 23(3):197
- Cowin S (2000) How is a tissue built? *J Biomech Eng* 122:553
- Cowin S (2004) Tissue growth and remodeling. *Ann Rev of Biomed Eng* 6(1):77–107
- Curtis A, Riehle M (2001) Tissue engineering: the biophysical background. *Phys in Med and Biol* 46:47–65
- Drew D, Segel L (1971) Averaged equations for two-phase flows. *Studies in Appl Math* 50:205–231
- Franks S, King J (2003) Interactions between a uniformly proliferating tumour and its surroundings: uniform material properties. *Math Med Biol* 20:47–89
- Freed L, Vunjak-Novakovic G (1998) Culture of organized cell communities. *Advanced Drug Delivery Rev* 33:15–30
- Freed L, Vunjak-Novakovic G, Biron R, Eagles D, Lesnoy D, Barlow S, Langer R (1994) Biodegradable polymer scaffolds for tissue engineering. *Nat Biotech* 12(7):689–693
- Fung Y (1991) What are residual stresses doing in our blood vessels? *Ann Biomed Eng* 19:237–249
- Haider M, Olander J, Arnold R, Marous D, McLamb A, Thompson K, Woodruff W, Haugh J (2010) A phenomenological mixture model for biosynthesis and linking of cartilage extracellular matrix in scaffolds seeded with chondrocytes. *Biomech Model Mechanobiol* pp 1–10
- Haj AE, Minter S, Rawlinson S, Suswillo R, Lanyon L (1990) Cellular responses to mechanical loading in vitro. *J Bone and Min Res* 5(9):923–32
- Han Y, Cowin S, Schaffler M, Weinbaum S (2004) Mechanotransduction and strain amplification in osteocyte cell processes. *Proc Nat Acad of Sci* 101(47):16,689–16,694
- Holzappel G, Ogden R (2006) *Mechanics of biological tissue*. Springer-Verlag, Berlin
- Kelly D, Prendergast P (2003) Effect of a degraded core on the mechanical behaviour of tissue-engineered cartilage constructs: a poro-elastic finite element analysis. *Med Biol Eng and Comp* 42:9–13
- Klein-Nulend J, Roelofsens J, Sterck J, Semeins C, Burger E (1995) Mechanical loading stimulates the release of transforming growth factor- $\beta$  activity by cultured mouse calvariae and periosteal cells. *Journal of Cell Physiology* 163(1):115–119
- Landman K, Please C (2001) Tumour dynamics and necrosis: Surface tension and stability. *IMA J of Math Appl in Med and Biol* 18(2):131–158
- Lemon G, King J (2007) Multiphase modelling of cell behaviour on artificial scaffolds: effects of nutrient depletion and spatially nonuniform porosity. *Math Med Biol* 24(1):57
- Lemon G, King J, Byrne H, Jensen O, Shakesheff K (2006) Multiphase modelling of tissue growth using the theory of mixtures. *J Math Biol* 52(2):571–594
- Lewis M, Macarthur B, Malda J, Pettet G, Please C (2005) Heterogeneous proliferation within engineered cartilaginous tissue: the role of oxygen tension. *Biotech and Bioeng* 91(5):607–15
- Lubkin S, Jackson T (2002) Multiphase Mechanics of Capsule Formation in Tumors. *J Biomech Eng* 124:237
- Martin I, Wendt D, Heberer M (2004) The role of bioreactors in tissue engineering. *Trends in Biotechnol* 22(2):80–86
- Nikolovski J, Mooney D (2000) Smooth muscle cell adhesion to tissue engineering scaffolds. *Biomater* 21(20):2025–2032
- O'Dea R, Waters S, Byrne H (2008) A two-fluid model for tissue growth within a dynamic flow environment. *Eur J Appl Math* 19(641):607–634

- O'Dea R, Waters S, Byrne H (2010) A three phase model for tissue construct growth in a perfusion bioreactor. *J Math Med Biol* 27(2):95–127
- O'Dea R, Waters S, Byrne H (2011) Modelling tissue growth in bioreactors: a review. In: Geris L (ed) *Computational Modeling in Tissue Engineering*, Springer-Verlag
- Osborne J, Whiteley J (2010) A numerical method for the multiphase viscous flow equations. *Comput Methods Appl Mech Engrg* 199:3402–3417, doi:10.1016/j.cma.2010.07.011
- Osborne J, O'Dea R, Whiteley J, Byrne H, Waters S (2010) The influence of bioreactor geometry and the mechanical environment on engineered tissues. *J Biomech Eng* 132(5), doi: 10.1115/1.4001160
- Preziosi L, Tosin A (2009) Multiphase and multiscale trends in cancer modelling. *Math Model Nat Phenom* 4(3):1–11
- Roelofsen J, Klein-Nulend J, Burger E (1995) Mechanical stimulation by intermittent hydrostatic compression promotes bone-specific gene expression in vitro. *J Biomech* 28(12):1493–1503
- Roose T, Neti P, Munn L, Boucher Y, Jain R (2003) Solid stress generated by spheroid growth estimated using a poroelasticity model. *Microvascular Res* 66:204–212
- Sanz-Herrera J, García-Aznar J, Doblaré M (2008) On scaffold designing for bone regeneration: A computational multiscale approach. *Acta Biomater* Online PrePrint
- Sipe J (2002) *Tissue Engineering and Reparative Medicine*. Ann of the New York acad of Sci 961:1–9
- Skalak R, Zargaryan S, Jain R, Netti P, Hoger A (1996) Compatibility and the genesis of residual stress by volumetric growth. *J Math Biol* 34:889–914
- Urban J (1994) The chondrocyte: a cell under pressure. *Rheumat* 33(10):901–908
- VonNeumann J, Richtmyer R (1950) A method for the numerical calculation of hydrodynamic shocks. *J Appl Phys* 21:232
- Wang Q, Nguyen B, Thomas C, Zhang Z, El Haj A, Kuiper N (2010) Molecular profiling of single cells in response to mechanical force: comparison of chondrocytes, chondrons and encapsulated chondrocytes. *Biomater* 31(7):1619–1625
- Wilson D, King J, Byrne H (2007) Modelling scaffold occupation by a growing, nutrient-rich tissue. *Math Models Methods Appl Sci* 17:1721
- Wu L, Ding J (2004) In vitro degradation of three-dimensional porous poly(d,l-lactide-co-glycolide) scaffolds for tissue engineering. *Biomater* 25(27):5821–5830
- Yang Y, El Haj A (2006) Biodegradable scaffolds – delivery systems for cell therapies. *Expert Opin Biol Ther* 6(5):485–498
- You J, Yellowley C, Donahue H, Zhang Y, Chen Q, Jacobs C (2000) Substrate deformation levels associated with routine physical activity are less stimulatory to bone cells relative to loading-induced oscillatory fluid flow. *Journal of Biomechanical Engineering* 122:377–393
- You L, Cowin S, Schaffler M, Weinbaum S (2001) A model for strain amplification in the actin cytoskeleton of osteocytes due to fluid drag on pericellular matrix. *J Biomech* 34(11):1375–86
- Yourek G, Al-Hadlaq A, Patel R, McCormick S, Reilly G, Mao J (2004) Nanophysical properties of living cells. In: Strosio MA, Dutta M, He B (eds) *Biological Nanostructures and Applications of Nanostructures in Biology, Bioelectric Engineering*, Springer US, pp 69–97



## RECENT REPORTS

04/12	Numerical studies of homogenization under a fast cellular flow.	Iyer Zygalakis
05/12	Solute transport within porous biofilms: diffusion or dispersion?	Davit Byrne Osborne Pitt-Francis Gavaghan Quintard
65/11	Adaptive Finite Element Method Assisted by Stochastic Simulation of Chemical Systems	Cotter Vejchodsky Erban
06/12	Effects of intrinsic stochasticity on delayed reaction-diffusion patterning systems	Woolley Baker Gaffney Maini Seirin-Lee
07/12	Axial Dispersion via Shear-enhanced Diffusion in Colloidal Suspensions	Griffiths Stone
08/12	Qualitative Analysis of an Integro-Differential Equation Model of Periodic Chemotherapy	Jaina Byrne
09/12	Modeling Stem/Progenitor Cell-Induced Neovascularization and Oxygenation	Jain Moldovan Byrne
10/12	Allee Effects May Slow the Spread of Parasites in a Coastal Marine Ecosystem	Krkošek Connors Lewis Poulin
11/12	Parasite spill-back from domestic hosts may induce an Allee effect in wildlife hosts	Krkošek Ashander Lewis
12/12	Modelling temperature-dependent larval development and subsequent demographic Allee effects in adult populations of the alpine butterfly <i>Parnassius smintheus</i>	Wheeler Bampfylde Lewis
13/12	Putting “space” back into spatial ecology	Fortin Peres-Neto Lewis
14/12	Wildlife disease elimination and density dependence	Potapova Merrill Lewis
15/12	Spreading Speed, Traveling Waves, and Minimal Domain Size in Impulsive Reaction-diffusion Models	Lewis Li
16/12	MCMC methods for functions modifying old algorithms to make them faster	Cotter Roberts Stuart White



18/12	A note on oblique water entry	Moore Howison Ockendon Oliver
19/12	Calculus on surfaces with general closest point functions	März Macdonald
20/12	Multiple equilibria in a simple elastocapillary system	Taroni Vella
21/12	Multiphase modelling of vascular tumour growth in two spatial dimensions	Hubbard Byrne
22/12	Chebfun and Numerical Quadrature	Hale Trefethen
23/12	Moment-based formulation of NavierMaxwell slip boundary conditions for lattice Boltzmann simulations of rarefied flows in microchannels	Reis Dellar
24/12	Correspondence between one- and two-equation models for solute transport in two-region heterogeneous porous media	Davit Wood Debenest Quintard
25/12	Rolie-Poly fluid flowing through constrictions: Two distinct instabilities	Reis Wilson
26/12	Age related changes in speed and mechanism of adult skeletal muscle stem cell migration	Collins-Hooper Woolley Dyson Patell Potter Baker Gaffney Maini Dash Patel

**Copies of these, and any other OCCAM reports can be obtained from:**

**Oxford Centre for Collaborative Applied Mathematics  
Mathematical Institute  
24 - 29 St Giles'  
Oxford  
OX1 3LB  
England**

[www.maths.ox.ac.uk/occam](http://www.maths.ox.ac.uk/occam)